# Bottom-Up Fabrication of Sulfur-Doped Graphene Films Derived from Sulfur-Annulated Nanographene for Ultrahigh Volumetric Capacitance Micro-Supercapacitors

Zhong-Shuai Wu,*[,†] Yun-Zhi Tan,[‡] Shuanghao Zheng,[†,§,#] Sen Wang,[†,#] Khaled Parvez,[∥] Jieqiong Qin,[†,#] Xiaoyu Shi,[†,§] Chenglin Sun,[†,#] Xinhe Bao,[†,§] Xinliang Feng,*[,¶] and Klaus Müllen,*[,¥]

[†]Dalian National Laboratory for Clean Energy, Dalian Institute of Chemical Physics, Chinese Academy of Sciences 457 Zhongshan Road, Dalian 116023, China

[‡]State Key Laboratory for Physical Chemistry of Solid Surfaces and Department of Chemistry College of Chemistry and Chemical Engineering, Xiamen University, 422 Siming South Road, Xiamen, 361005, China

[§]State Key Laboratory of Catalysis, Dalian Institute of Chemical Physics, Chinese Academy of Sciences, 457 Zhongshan Road, Dalian 116023, China

[#]University of Chinese Academy of Sciences, 19 A Yuquan Rd, Shijingshan District, Beijing, 100049, China

[∥]School of Chemistry, University of Manchester, Oxford Road, Manchester M13 9PL, UK

[¶]Center for Advancing Electronics Dresden (cfaed) & Department of Chemistry and Food Chemistry, Technische Universität Dresden, Mommsenstraβe 4, 01062 Dresden, Germany

[¥]Max-Planck-Institut für Polymerforschung, Ackermannweg 10, 55128 Mainz, Germany

Supporting Information Placeholder

**ABSTRACT:** Heteroatom doping of nanocarbon films can efficiently boost the pseudocapacitance of micro-supercapacitors (MSCs), however, wafer-scale fabrication of sulfur-doped graphene films with a tailored thickness and homogeneous doping for MSCs remains a great challenge. Here we demonstrate the bottom-up fabrication of continuous, uniform, ultrathin sulfur-doped graphene (SG) films, derived from the peripherical tri-sulfur-annulated hexa-*peri*-hexabenzocoronene (SHBC), for ultrahigh-rate MSCs (SG-MSCs) with landmark volumetric capacitance. The SG film was prepared by thermal annealing of the spray-coated SHBC-based film, with assistance of a thin Au protecting layer, at 800 $^{o}$C for 30 min. SHBC with twelve phenylthio groups decorated at the periphery is critical as precursor for the formation of the continuous and ultrathin SG film, with a uniform thickness of ~10.0 nm. Notably, the as-produced all-solid-state planar SG-MSCs exhibited a highly stable pseudocapacitive behavior with an volumetric capacitance of ~582 F cm$^{-3}$ at 10 mV s$^{-1}$, excellent rate capability with a remarkable capacitance of 8.1 F cm$^{-3}$ even at an ultrahigh rate of 2000 V s$^{-1}$, ultrafast frequency response with a short time constant of 0.26 ms, and ultrahigh power density of ~1191 W cm$^{-3}$. It is noteworthy that these values obtained are among the best values for carbon-based MSCs reported to date.

## ■ INTRODUCTION

The current development of flexible and wearable electronics concentrates on the continuous miniaturization and diversified integration of micro-scale power sources.[1-4] The conventional energy storage devices such as lithium ion batteries and supercapacitors, however, are usually configured with sandwich-like stacked geometries which poorly miniaturize in size and are not well compatible with planar integrated circuits on one single substrate.[5-7] In this regard, the emerging planar micro-supercapacitor (MSC) device components, including two electrodes, separator, electrolyte, and current collectors of MSCs are readily constructed on one single substrate. Furthermore, the MSCs possess desirable merits of ultrahigh power delivery, outstanding rate capability, and high-frequency response.[8-10] Notable efforts have been devoted to the development of advanced thin-film electrode materials of nanostructured carbon materials, metal oxides, and conducting polymers for MSCs.[11,12] The available metal oxides, e.g., $RuO_2$,[13] $MnO_2$,[14] $Ni(OH)_2$,[15] CoO,[16] and conducting polymers, e.g., polyaniline,[17] polypyrrole,[18] generally show high volumetric capacitance of 300~800 F cm$^{-3}$, but suffer from limited power delivery, slow frequency response and short cycling stability because of poor electrode kinetics.[19,20] As a consequence, "nanocarbons", including activated carbon (AC),[21,22] carbide-derived carbon (CDC),[8] onion-like carbon (OLC),[23] carbon nanotubes (CNTs),[24] and graphene[25-30] appear as most promising candidates for MSCs.

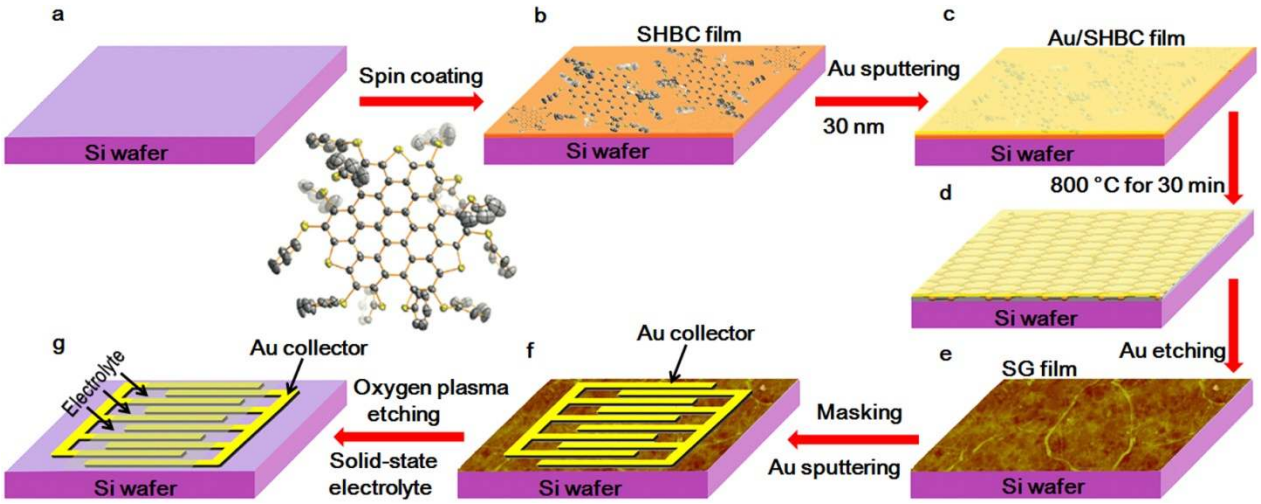


**Figure 1.** Schematic illustration of SHBC-derived SG films for planar MSCs on a $Si/SiO_2$ wafer. (a) Spin-coating of the SHBC solution on surface-modified silicon with oxygen plasma treatment. (b) Sputtering Au with a thickness of 30 nm on the SHBC film. (c) Thermal annealing at 800 °C for 30 min. (d) Au etching by a $KI/I_2$ aqueous solution. (e) Masking micropatterns and deposition of gold current collector. (f) Oxygen plasma etching and drop casting of $H_2SO_4$/PVA gel electrolyte on interdigitated fingers. (g) All-solid-state SG-MSCs obtained after solidification of gel electrolyte.

The incorporation of single or dual heteroatoms (e.g., N,[31-33] B,[34-36] P,[37-39] S,[40-42] O[43]) into the nanocarbons is a practical strategy to considerably enhance the capacitance through additional Faradaic reactions generally called pseudocapacitance effects.[44,45] Special emphasis is given to sulfur doping. Sulfur has a similar electronegativity (2.58) as carbon (2.55) in the graphitic layers,[46] which is also effective in modifying the electronic arrangement of graphitic lattice, as doped by larger electronegative nitrogen (3.04).[47] Recent theoretical and experimental studies have proven that the presence of sulfur heteroatoms could substantially modify spin densities on graphene,[47,48] producing significantly improved materials for supercapacitors.[40,41] In particular, C-S bonds at the edge or near defects are important active sites, which greatly influence the charging of the electrical double layer and eventually facilitate the pseudocapacitance behavior.[42] In addition, bottom-up synthesis is a reliable strategy towards high yielding production of defect-free molecular graphene (≤ 5 nm), nanographene (5-500 nm) and macrographene (≥500 nm) through controlled chemical reaction or thermolysis of structurally-defined precursors, e.g., polycyclic aromatic hydrocarbons.[49] With this approach, the structure of the precursor together with chemical or thermal reactions will determine the structure of the product, which is critical for the growth and integration of structurally-defined large graphene and graphene-based materials,[49] showing exciting properties for electronic, optoelectronic and energy devices.[50] Although planar MSCs based on nitrogen[51] and boron[52] doped carbon films have been reported, bottom-up fabrication of thin sulfur-doped carbon films with a tailored thickness and homogeneous doping for MSCs has remained elusive.

Herein we develop the bottom-up fabrication of continuous, uniform, ultrathin sulfur-doped graphene (SG) films, derived from the peripherical tri-sulfur-annulated hexa-*peri*-hexabenzocoronene (SHBC, nanographene), for ultrahigh volumetric capacitance MSCs (denoted as SG-MSCs). The wafer-scale SG film with a uniform thickness of ~10.0 nm was produced by thermal annealing of the spray-coated SHBC-based film under a thin Au protecting layer, at 800 °C for 30 min. Remarkably, the as-produced all-solid-state planar SG-MSCs presented outstanding pseudocapacitive behavior with unprecedented volumetric capacitance of ~582 F $cm^{-3}$ (10 mV $s^{-1}$), excellent rate capability with a remarkable capacitance of 8.1 F $cm^{-3}$ even at an ultrahigh rate of 2000 V $s^{-1}$, an extremely short time constant of 0.26 ms, and ultrahigh power density of ~1191 W $cm^{-3}$. It is highlighted that these values obtained are among the best values for carbon-based MSCs reported to date.

## ■ RESULTS AND DISCUSSION

**Fabrication of SG-MSCs.** Figure 1 schematically depicts the stepwise fabrication of the planar SG-MSCs on a $Si/SiO_2$ wafer. First, the SHBC with twelve phenylthio groups decorated at the periphery was synthesized by thiolation of perchlorinated HBC (Figure S1 in Supporting Information), as described in our previous work.[53,54] Then, a thin SHBC film was obtained by spin-coating a SHBC dispersion (0.5 mg $mL^{-1}$, Figure S2a) on an oxygen plasma treated silicon wafer (Figure 1a,b). After sputtering a thin Au layer with a thickness of 30 nm (Figure 1c, Figure S2b), the SHBC film was thermally treated at 400 °C for 30 min (denoted as SHBC400), and then at 800 °C for 30 min (Figure 1d). It should be mentioned that the surface coverage of thin Au layer is helpful for the adsorption of cleaved sulfurs of twelve thiol groups of HBC molecule on the gold surface via the S-Au bonds,[55] and simultaneous reorganization of these S-terminated HBC molecules via the cleavage of C-S bonds in phenylthio groups to form a surface-attached film. Further, the Au layer can be regarded as the two-dimensional (2D) catalytic cover,[56,57] which provides a 2D confinement effect for the continuous growth of SHBC-derived SG film during annealing process. As expected, a wafer-scale film could not be obtained without a confining Au layer and without thermal annealing at 400 °C (Figure S3), or when replacing the precursor SHBC by pristine HBC (hexa-tert-butyl-hexa-peri-hexabenzocoronene), without thiol groups decorated at the periphery (Figure S4). After removing the Au layer by etching

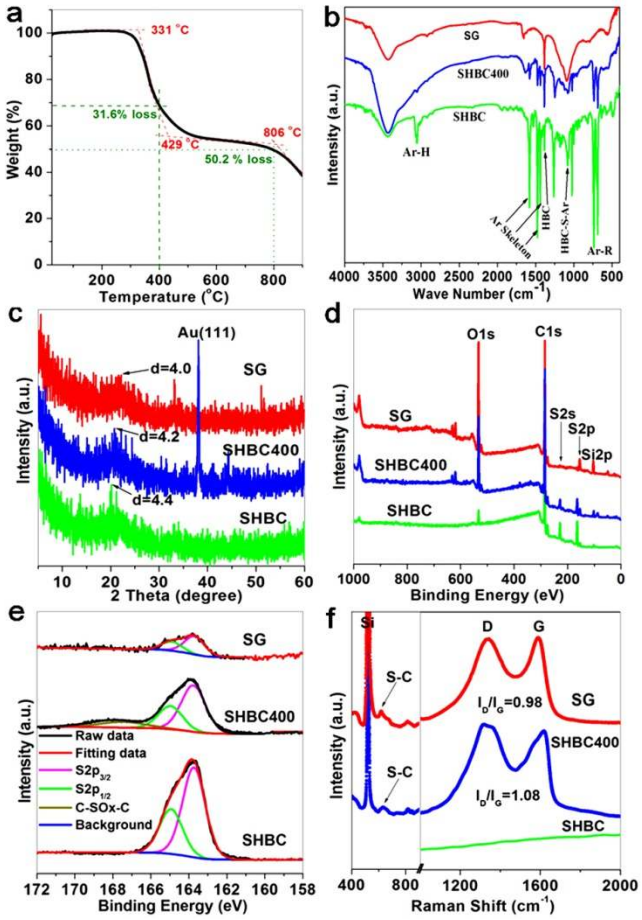


**Figure 2.** Structural characterization of SG, SHBC400 and SHBC films. (a) TGA curve of SHBC measured from 25 to 900 °C in nitrogen atmosphere with a heating rate of 5 °C/min. (b) FT-IR spectra (Ar stands for aromatic core or benzene ring), (c) XRD patterns, (d) overview XPS spectra, (e) high-resolution S2p XPS spectra, and (f) Raman spectra of SG, SHBC400 and SHBC films.

with a KI/$I_2$ solution (Figure 1e, Figure S2c), the SG-based interdigitated microelectrode patterns were created through the deposition of gold current collectors, followed by oxidative etching in an oxygen plasma (Figure 1f,g). Finally, a polymer gel electrolyte of $H_2SO_4$/polyvinyl alcohol ($H_2SO_4$/PVA) was drop-cast onto the interdigitated fingers, and the planar SG-MSCs were obtained after solidification overnight (Figure 1g).

**Characterization of SG Film.** The structural evolution of SG films, SHBC400 and SHBC, was evaluated based on thermogravimetric analysis (TGA), Fourier transform infrared (FT-IR) spectroscopy, X-ray diffraction (XRD) patterns, X-ray photoelectron spectroscopy (XPS) and Raman spectra (Figure 2). In TGA curve (Figure 2a), SHBC showed a major mass reduction of approximately 50.2 wt% up to 800 °C, which was basically close to the theoretical weight loss ~50.3 wt% of twelve phenyl groups. This is suggested the cleavage of C-S bonds in phenylthio groups. Note that the aromatic HBC units were thermally stable until 800 °C, in accordance with the literature.[58] The loss of the phenyl groups from SHBC at 800 °C was further identified by FT-IR (Figure 2b). SHBC exhibited characteristic bands, including 3046 $cm^{-1}$ for the C-H stretching vibration,[58] 1580, 1527, 1476 and 1437 $cm^{-1}$ for benzene ring stretching vibrations, 686 $cm^{-1}$ for the C-H deformation vibration of the phenyl groups,[58] and 736 $cm^{-1}$ for out-of-plane bending mode of the aromatic core,[57] respectively. However, with increased temperature, it was observed that the total intensities of these bands were substantially weakened for SHBC400 due to the part decomposition of phenyl groups, and disappeared for the SG film, indicating the completed removal of phenyl groups annealed at 800 °C. Moreover, two peaks at 1384 $cm^{-1}$ and 1098 $cm^{-1}$, corresponding to the vibrations of C-C bonds and collective ring breathing mode of the aromatic HBC-S core,[59] respectively, confirmed the intact HBC-S moieties after annealing at 800 °C.

The XRD pattern displayed a broad diffraction peak (002) at 20.13° for SHBC film and 20.76° for the SHBC400 film, corresponding to a d-spacing of 4.4 Å and 4.2 Å, respecitively. After annealing at 800 °C, the characteristic (002) peak shifted to a larger angle of 22.18° and one noted a decreased d-spacing of 4.0 Å (Figure 2c), suggestive of the enhanced graphitization of SG film upon annealing process. XPS characterization was performed to probe the chemical composition of the SG, SHBC400, and SHBC films (Figure 2d,e). From the full XPS spectra (Figure 2d), the characteristic peaks of C1s and S2p were observed. The SG film gave a sulfur doping content of 1.5 at% while the pristine SHBC and SHBC400 contained ~11.6 at % and ~7.1 at% sulfur moieties, respectively. High-resolution S2p XPS spectra of SG, SHBC400 and SHBC films differ only in the intensity of the C-S peaks reflecting a different content of C-S bonds. All S2p XPS spectra can be deconvoluted into two distinct peaks featuring the S-C bond at 165.0 and 163.7 eV (Figure 3d), which are identified as

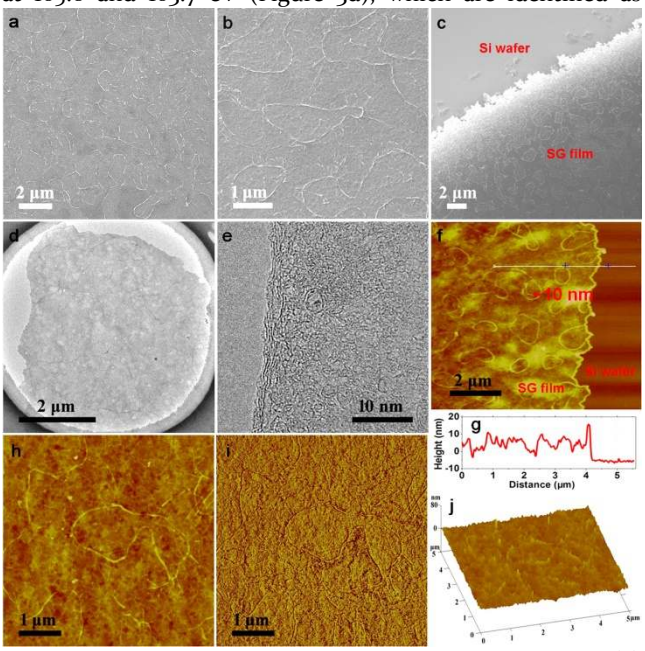


**Figure 3.** Surface morphology of SHBC-derived SG films. (a) Low-magnification and (b) high-magnification SEM images of SG film. (c) SEM image of the finger edges of the SG film, created by the oxidative etching, showing an edge resolution of around 2 μm. (d) TEM and (e) HRTEM images of the SG film. (f) AFM height image and (g) height profile of the edge of the SG film, with an average thickness of ~10 nm. (h-j) AFM (h) height image, (i) phase image and (j) 3D surface plot of the top-view of the SG film.

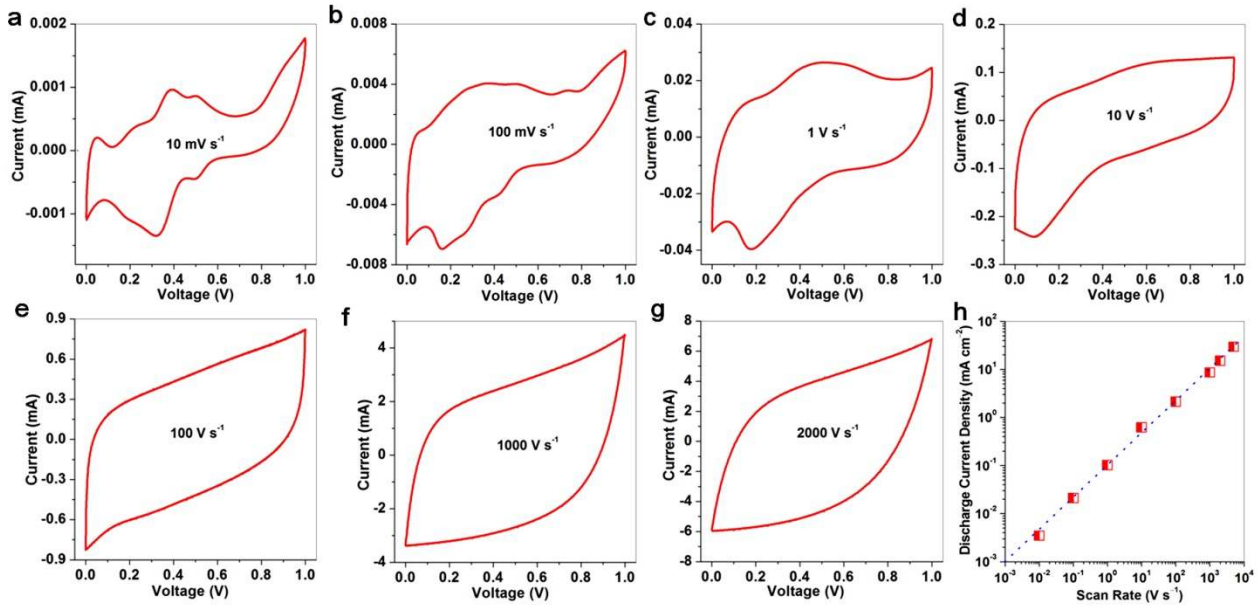


**Figure 4.** Electrochemical comparison of SG-MSCs. (a-g) CV curves of SG-MSCs measured at different scan rates of (a) 0.01, (b) 0.1, (c) 1, (d) 10, (e) 100, (f) 1000, and (g) 2000 V $s^{-1}$. (h) Plot of the discharge current as a function of the scan rate for SG-MSCs. Linear dependence observed at 2000 $Vs^{-1}$ (blue dot line) suggests ultrahigh power delivery of SG-MSCs.

the spin-orbit coupling positions of $S2p_{1/2}$ and $S2p_{3/2}$, respectively.[42,47,60] For the SHBC400 film, the S2p XPS spectrum exhibited an additional component at 167~169 eV that was assigned to carbon bonded $SO_x$ species.[46,48] This resulted from the decomposition of the SHBC, in which the terminated sulfurs in S-HBC units might interact with oxygen atoms likely adsorbed on samples in air. Further, the bond of C-S (286.5 eV) in the C1s XPS spectrum of the SG film was also unraveled (Figure S5).[47,60] Raman spectra showed the representative broad D and G peaks for SHBC400 and SG film, indicative of the nature of a carbonized film (Figure 2f). The decreased $I_D/I_G$ ratio from 1.08 for SHBC400 to 0.98 for SG film accounted for an enhanced degree of graphitization,[61] which is good agreement with XRD result (Figure 2c). In addition, both SHBC and SHBC400 films had an extremely low value of <0.001 S $cm^{-1}$. Note that the low conductivity of SHBC400 film is ascribe to the partly decomposition of SHBC at 400 °C, consisting of the decomposed phenyl groups and intact HBC-S moieties. By contrast, the as-produced SG film exhibited high electrical conductivity of ~95 S $cm^{-1}$, measured by a standard four-point probe system. These results demonstrated the successful fabrication of an S-doped, conductive SG film derived from a sulfur-annulated nanographene with assistance of Au confinement layer.

The surface topography of the SHBC-derived SG film was further investigated by scanning electron microscopy (SEM), transmission electron microscopy (TEM) and atomic force microscopy (AFM) measurements (Figure 3, and Figure S6-S8). Low-magnification SEM (Figure 3a) and TEM (Figure 3d) images of the as-fabricated SG films were continuous and uniform over a large area. High-magnification SEM image (Figure 3b, c) disclosed the formation of the irregularly circular-shaped grain boundaries (Figure S6 and S7). High resolution TEM (HRTEM) image displayed the existence of discontinuous graphitic stacked layers (Figure 3e and Figure S7). The AFM height image and phase images as well as 3D surface plot confirmed irregularly circular-shaped grain boundaries and a relatively uniform flat morphology with a typical thickness of ~10.0 nm for the SG film (Figure 3f-j, Figure S8). The energy dispersive X-ray (EDX) spectrum and mapping analysis further demonstrated the uniform doping of sulfur into the SG film (Figure S9), identical to the XPS results (Figure 2d,e). The resulting SG film exhibited a low average surface roughness of $R_a$ <2.5 nm for the whole measurement area (Figure 3i, j).

**Electrochemical Characterization of SG-MSCs**. The electrochemical performance of SG-MSCs was first examined by cyclic voltammetry (CV) at scan rates ranging from 0.01 to 2000 V $s^{-1}$ (Figure 4a-g). At low scan rates from 10 to 100 mV $s^{-1}$, the SG-MSCs showed a pronounced pseudocapacitive effect with three pairs of strong redox peaks (Figure 4a, b), supporting the importance of sulfur-doping in carbon films. With increasing scan rate, the CV curves revealed a gradual transition from the pseudocapacitive to the electric double-layer capacitive behavior with a nearly rectangular CV shape (Figure 4c-f). Remarkably enough, our SG-MSCs possessed ultrafast charging and discharging capability, and could be operated at ultrahigh scan rates of up to 2000 V $s^{-1}$ (Figure 4g, Figure S10). which is three orders of magnitude higher than that of conventional supercapacitors, and much higher than those of the reported high-power MSCs (Table S1), e.g., onion-like carbon (OLC, 200 V $s^{-1}$),[23] electrochemically rGO (ErGO, 400 V $s^{-1}$),[62] and methane plasma reduced graphene (MPG, 1000 V $s^{-1}$),[27] and vertically aligned CNTs (1000 V $s^{-1}$).[63] Furthermore, a linear dependence of the logarithmic discharge current upon scan rate was identified up to 2000 V $s^{-1}$ (Figure 4h), characteristic of ultrahigh instantaneous power.

The evolution of the areal capacitance and volumetric capacitance of SG-MSCs with scan rate is shown in Figure 5a. The areal capacitance and volumetric capacitance of SG film for MSCs recorded at 10 mV $s^{-1}$ were calculated to be ~553 μF $cm^{-2}$ and ~582 F $cm^{-3}$, respectively, both of which are much higher than those of films of undoped reduced graphene (RG, ~208 μF $cm^{-2}$, ~245 F $cm^{-3}$), nitrogen-doped graphene

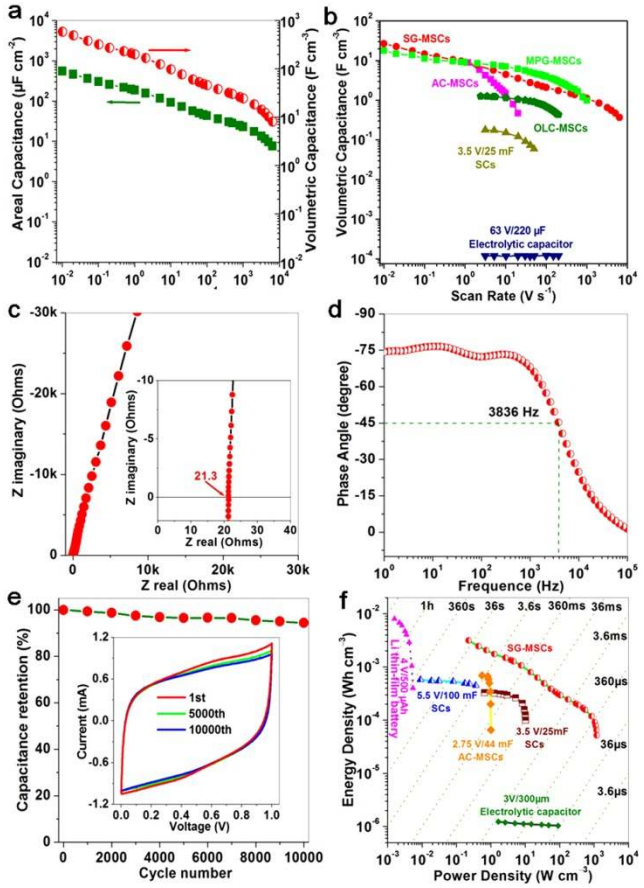


**Figure 5.** Electrochemical characterization of SG-MSCs. (a) Evolution of areal capacitance (left) and volumetric capacitance versus scan rate of SG film for SG-MSCs (based on single electrode). (b) Comparison of the volumetric capacitance versus scan rate of SG film for SG-MSCs (based on the whole device) with MPG-MSCs,[27] AC-MSCs, OLC-MSCs,[23] 3.5 V/25 mF supercapacitors (SCs), and 63 V/220 μF electrolytic capacitor.[23] (c) Complex plane plot of the impedance of SG-MSCs. Inset: magnified plot of the high-frequency region. (d) Impedance phase angle as a function of frequency of SG-MSCs. The -45° phase angle was observed at 3836 Hz, demonstrative of the fast accessibility of the ions in SG-MSCs. (e) Cycling stability of SG-MSCs. Inset: the 1st, 5000th, and 10000th CV curves of SG-MSCs tested at 200 V $s^{-1}$. (f) Ragone plot of SG-MSCs in comparison with the commercially available lithium thin-film batteries (4V/500 μAh), electrolytic capacitor (3V/300 μF), AC-MSCs (2.75V/44 mF), supercapacitors (SCs, 3.5 V/25 mF, and 5.5 V/100 mF), suggestive of simultaneously high energy and power densities of SG-MSCs.

(NG, ~361 μF $cm^{-2}$, ~425 F $cm^{-3}$), and boron/nitrogen co-doped graphene (BNG, ~415 μF $cm^{-2}$, ~488 F $cm^{-3}$) for MSCs.[51] It has appeared that heteroatom doping (e.g., N, B, S, and N/B) in nanocarbons is highly effective for the enhancement of supercapacitor performance because of the pseudocapacitive effect and the improvement of the interface wettability.[33] The pronounced enhancement provided by S doping furnishing multiple robust redox peaks in our SG-MSCs has never been disclosed previously. Further, the cell volumetric capacitance of SG-MSCs is well comparable to those of the state-of-the-art MSCs, e.g., MPG-MSCs,[27] AC-MSCs,[23] OLC-MSCs,[23] and much higher than that of commercially available supercapacitors (3.5 V/25 mF), and three orders of magnitude higher than that of electrolytic capacitors (63 V/220 μF),[23] as shown in Fig. 5b. Moreover, our SG-MSCs can still offer a significant cell capacitance of ~8.1 F $cm^{-3}$ even at ultrahigh rate of 2000 V $s^{-1}$ (Fig.5b).

Electrochemical impedance spectroscopy (EIS) of the SG-MSCs exhibits a closed 90° slope without a charge transport semicircle at high frequency (Fig. 5c), a vertical line intersection with the real axis at low frequency, and a low equivalent series resistance of 21.3 Ω (inset in Fig. 5c), suggestive of ultrafast ion diffusion in such a microdevice.[64] The dependence of the phase angle on the frequency for SG-MSCs (Fig. 5d) furnished a high characteristic frequency $f_o$ of 3836 Hz at the phase angle of -45°. Correspondingly, the relaxation time constant $\tau_o$ ($\tau_o$=1/$f_o$) was calculated to be only 0.26 ms for SG-MSCs. This value is three orders of magnitude lower than that of conventional AC electrical double layer capacitors (EDLCs, ~1 s),[64] much shorter than those of high-power supercapacitors and MSCs based on liquid-mediated graphene (0.2~0.73 s),[65] OLC (26 ms),[23] graphene/PH1000 (1.0~2.9 ms),[66] sulfuric acid treated poly(3,4-ethylenedioxythiophene):poly(styrenesulfonate) (0.588 ms),[67] MPG (0.28 ms),[27] ErGO (0.17~1 ms),[62] and vertically oriented graphene (0.067 ms).[64] In addition, the cycling stability of SG-MSCs was measured for 10000 times at a scan rate of 200 V $s^{-1}$ (Fig.5e), maintaining ~95.0% of the initial capacitance (Fig.5d).

The Ragone plot in Fig. 5f compares the volumetric performance of our SG-MSCs with those of commercially available energy-storage devices.[68] Our microdevice exhibits a volumetric energy density $E_{device}$ of ~3.1 mWh $cm^{-3}$, which is about ten times higher than those of commercially available supercapacitors (3.5 V/25 mF[23] and 5.5 V/100 mF, <1 mWh $cm^{-3}$), AC-MSCs (2.75V/44 mF), and well comparable to lithium thin-film batteries (4 V/500 μAh, 0.3~10 mWh $cm^{-3}$).[4] This energy density value is also higher than those of recently reported thin film MSCs, e.g., MPG (2.5 mWh $cm^{-3}$),[27] NG (2.96 mWh $cm^{-3}$),[51] BNG (3.4 mWh $cm^{-3}$),[51] laser scribed graphene (2.0 mWh $cm^{-3}$),[26] OLC (1.6 mWh $cm^{-3}$),[23] laser written graphene (4.0 mWh $cm^{-3}$) (Table S1).[25] Remarkably enough, our SG-MSCs offered a power density $P_{device}$ of ~1191 W $cm^{-3}$, which is the highest value reported so far, and comparable to that of high-power electrolytic capacitors ($10^1$~$10^3$ W $cm^{-3}$).[69]

## ■ CONCLUSION

In summary, we have demonstrated the first case of bottom-up, wafer-scale production for highly continuous, uniform, ultrathin SG films derived from a sulfur-decorated nanographene. This fabrication strategy using nanographene molecule as precursor, with assistance of a thin Au layer as 2D confining cover, provided a new scaffold for constructing large-area carbon films with uniform S doping, high conductivity and expanded interlayer spacing for high-performance MSCs. The films showed an unprecedented volumetric capacitance of ~582 F $cm^{-3}$, remarkable scan rate of 2000 V $s^{-1}$, ultrafast frequency response with a time constant of 0.26 ms, and ultrahigh power density of ~1191 W $cm^{-3}$. The as-produced SG film will offer numerous opportunities as an outstanding carbon-based material for electrochemical energy storage and conversion systems, such as metal-free oxygen reduction catalysts,[47, 61] Li-S batteries, and sensors.

## ■ EXPERIMENTAL SECTION

**Preparation of SG films.** The precursor of SHBC was first synthesized by thiolation of perchlorinated HBC, as described in our previous work.[53,54] Then, a stable SHBC dispersion of 0.5 mg/mL in dichloromethane was dissolved by sonication for 10 min, and subsequently spin-coated (2000 rpm, 60 s; Headway Research Inc.) on the oxygen plasma-treated silicon wafer (single size polished, 300 nm $SiO_2$ layer, Si-Mat) using 300 W rf power for 10 min (Plasma System 200-G, Technics Plamsa GmbH), and the spin-coating steps were repeated several times until the desirable SHBC film thickness was achieved. Afterwards, 40 nm Au protecting layer (Premion, 99.9985% metals basis, Alfa Aesar) was thermally evaporated (EDWARDS FL400) on the SHBC film with a rate of ~1.0 Å $s^{-1}$ and chamber pressure of ~2 x $10^{-6}$ Torr. With assistance of Au layer, the SHBC films were thermally annealed first at 400 $^{o}$C for 30 min, and then 800 $^{o}$C for 30 min, with a heating rate of ~5 $^{o}$C/min, by an AIXTRON furnace (Nanoinstruments Black Magic) in argon gas of 100 sccm. After the removal of Au layer etching by a $KI/I_2$ aqueous solution, the SG films were readily produced for further characterization and device manufacturing.

**Fabrication of SG-MSCs.** To fabricate the SG-MSCs, 30 nm gold was first thermally evaporated (EDWARDS FL400) on the SG film with a rate of ~1.0 Å $s^{-1}$ and chamber pressure of ~2 x $10^{-6}$ Torr through a home-made 30-interdigitated finger mask (widths of 210 μm, interspaces of 70 μm). After that, the electrode micro-patterns of SG film on Si wafer were created by oxidative etching of the exposed SG film in an $O_2$-plasma cleaner with 20 sccm $O_2$ flow for 90~150 s and 200 W rf power (Plasma System 200-G, Technics Plamsa GmbH). Afterwards, $H_2SO_4$/PVA gel electrolyte was slowly drop-casted onto the surface of interdigitated fingers and solidified overnight. Finally, the all-solid-state planar SG-MSCs were obtained. The gel electrolyte was prepared by mixing 3 g PVA and 3 g $H_2SO_4$ into 30 ml DI water, and heated at 80 °C for 1 h under stirring.

**Characterization.** Materials characterization were carried out by SEM (Gemini 1530 LEO), optical microscopy, AFM (Veeco Dimension 3100), surface profiler (KLA Tencor P-16+), XRD (SEIFERT XRD 3000 TT Bragg-Brentano diffractometer with Cu Ka radiation between 10° and 60° and an incident wavelength of 0.15418 nm), FT-IR (Nicolet iS50), TGA (STA 449 F3, from 25 to 800 $^{o}$C with a heating rate of 5 $^{o}$/min in nitrogen gas), Raman spectra (Bruker, 532 nm) and XPS (Omicron Multiprobe equipped with the monochromatic Al $K_\alpha$ source, electron analyzer resolution of 0.9 eV). For TEM characterization, the SG film was delaminated from the $SiO_2$/Si wafer in the HF solution (40%), and rinsed with deionized water three times. After that, the delaiminated SG film was carefully transferred into Cu grids. The electrical conductivity of the SG film was measured by a standard four-point probe system with a Kiethley 2700 Multimeter. The electrochemical properties was examined by CV at the scan rates of 0.01~5000 V $s^{-1}$, galvanostatic charge and discharge profiles at different current density, and EIS recorded in the frequency range of 1~100 kHz with a 5 mV ac amplitude, using a CHI 760D electrochemical workstation.

## ASSOCIATED CONTENT

This material is available free of charge via the Internet at http://pubs.acs.org.

Calculation of areal/volumetric capacitance, power/energy density, TEM, SEM, AFM and EDX analysis characterization of SG film, CVs of SG-MSCs, and Table S1. (PDF)

## AUTHOR INFORMATION

### Corresponding Author

* wuzs@dicp.ac.cn;
* xinliang.feng@tu-dresden.de;
* muellen@mpip-mainz.mpg.de

### Notes

The authors declare no competing financial interests.

## ACKNOWLEDGMENT

This work was financially supported by the National Natural Science Foundation of China (Grant 51572259), Ministry of Science and Technology of China (Grant 2016YBF0100100 and 2016YFA0200200), Natural Science Foundation of Liaoning Province (Grant 201602737), Thousand Youth Talents Plan of China, DICP (Grant Y5610121T3), China Postdoctoral Science Foundation (Grant 2016M601349), dedicated funds for methanol conversion from DICP, ERC Grant on 2DMATER, and EC under Graphene Flagship (No. CNECT-ICT-604391).

## REFERENCES

(1) LeMieux, M. C.; Bao, Z. N. *Nat. Nanotechnol.* **2008**, *3*, 585.
(2) Gates, B. D. *Science* **2009**, *323*, 1566.
(3) Liu, C.; Li, F.; Ma, L. P.; Cheng, H. M. *Adv. Mater.* **2010**, *22*, E28.
(4) Yu, D. S.; Goh, K.; Wang, H.; Wei, L.; Jiang, W. C.; Zhang, Q.; Dai, L. M.; Chen, Y. *Nat. Nanotechnol.* **2014**, *9*, 555.
(5) Wang, X.; Lu, X.; Liu, B.; Chen, D.; Tong, Y.; Shen, G. *Adv. Mater.* **2014**, *26*, 4763.
(6) Wen, L.; Li, F.; Cheng, H.-M. *Adv. Mater.* **2016**, *28*, 4306.
(7) Wan, S.; Peng, J.; Jiang, L.; Cheng, Q. *Adv. Mater.* **2016**, 28, 7862.
(8) Chmiola, J.; Largeot, C.; Taberna, P. L.; Simon, P.; Gogotsi, Y. *Science* **2010**, *328*, 480.
(9) Huang, P.; Lethien, C.; Pinaud, S.; Brousse, K.; Laloo, R.; Turq, V.; Respaud, M.; Demortière, A.; Daffos, B.; Taberna, P. L.; Chaudret, B.; Gogotsi, Y.; Simon, P. *Science* **2016**, *351*, 691.
(10) Beidaghi, M.; Gogotsi, Y. *Energy Environ. Sci.* **2014**, *7*, 867.
(11) Wu, Z.-S.; Feng, X.; Cheng, H.-M. *Natl Sci. Rev.* **2014**, *1*, 277.
(12) Wang, S.; Zheng, S. H.; Wu, Z.-S.; Sun, C. L. *Sci. Sin. Chim.* **2016**, *46*, 1.
(13) Ferris, A.; Garbarino, S.; Guay, D.; Pech, D. *Adv. Mater.* **2015**, *27*, 6625.
(14) Su, Z.; Yang, C.; Xie, B.; Lin, Z.; Zhang, Z.; Liu, J.; Li, B.; Kang, F.; Wong, C. P. *Energy Environ. Sci.* **2014**, *7*, 2652.
(15) Kurra, N.; Alhebshi, N. A.; Alshareef, H. N. *Adv. Energy Mater.* **2014**, *4*, 1401303.
(16) Zhu, Y. G.; Wang, Y.; Shi, Y.; Wong, J. I.; Yang, H. Y. *Nano Energy* **2014**, *3*, 46.
(17) Wang, K.; Zou, W. J.; Quan, B. G.; Yu, A. F.; Wu, H. P.; Jiang, P.; Wei, Z. X. *Adv. Energy Mater.* **2011**, *1*, 1068.
(18) Liu, S.; Gordiichuk, P.; Wu, Z.-S.; Liu, Z.; Wei, W.; Wagner, M.; Mohamed-Noriega, N.; Wu, D.; Mai, Y.; Herrmann, A.; Müllen, K.; Feng, X. *Nat. Commun.* **2015**, *6*, 8817.
(19) Zhai, Y.; Dou, Y.; Zhao, D.; Fulvio, P. F.; Mayes, R. T.; Dai, S. *Adv. Mater.* **2011**, *23*, 4828.
(20) Kurra, N.; Ahmed, B.; Gogotsi, Y.; Alshareef, H. N. *Adv. Energy Mater.* **2016**, 1601372.
(21) Wei, L.; Nitta, N.; Yushin, G. *ACS Nano* **2013**, *7*, 6498.

(22) Huang, H.-C.; Chung, C.-J.; Hsieh, C.-T.; Kuo, P.-L.; Teng, H. *Nano Energy* **2016**, *21*, 90.
(23) Pech, D.; Brunet, M.; Durou, H.; Huang, P. H.; Mochalin, V.; Gogotsi, Y.; Taberna, P. L.; Simon, P. *Nat. Nanotechnol.* **2010**, *5*, 651.
(24) Kim, S. K.; Koo, H. J.; Lee, A.; Braun, P. V. *Adv. Mater.* **2014**, *26*, 5108.
(25) Gao, W.; Singh, N.; Song, L.; Liu, Z.; Reddy, A. L. M.; Ci, L. J.; Vajtai, R.; Zhang, Q.; Wei, B. Q.; Ajayan, P. M. *Nat. Nanotechnol.* **2011**, *6*, 496.
(26) El-Kady, M. F.; Kaner, R. B. *Nat. Commun.* **2013**, *4*, 1475.
(27) Wu, Z.-S.; Parvez, K.; Feng, X. L.; Müllen, K. *Nat. Commun.* **2013**, *4*, 2487.
(28) Liu, Z.; Wu, Z.-S.; Yang, S.; Dong, R.; Feng, X.; Müllen, K. *Adv. Mater.* **2016**, *28*, 2217.
(29) Niu, Z. Q.; Zhang, L.; Liu, L. L.; Zhu, B. W.; Dong, H. B.; Chen, X. D. *Adv. Mater.* **2013**, *25*, 4035.
(30) Wu, Z.-K.; Lin, Z.; Li, L.; Song, B.; Moon, K.-s.; Bai, S.-L.; Wong, C.-P. *Nano Energy* **2014**, *10*, 222.
(31) Jeong, H. M.; Lee, J. W.; Shin, W. H.; Choi, Y. J.; Shin, H. J.; Kang, J. K.; Choi, J. W. *Nano Lett.* **2011**, *11*, 2472.
(32) Wen, Z.; Wang, X.; Mao, S.; Bo, Z.; Kim, H.; Cui, S.; Lu, G.; Feng, X.; Chen, J. *Adv. Mater.* **2012**, *24*, 5610.
(33) Lin, T.; Chen, I.-W.; Liu, F.; Yang, C.; Bi, H.; Xu, F.; Huang, F. *Science* **2015**, *350*, 1508.
(34) Yang, L. J.; Jiang, S. J.; Zhao, Y.; Zhu, L.; Chen, S.; Wang, X. Z.; Wu, Q.; Ma, J.; Ma, Y. W.; Hu, Z. *Angew. Chem. Int. Ed.* **2011**, *50*, 7132.
(35) Wang, D. W.; Li, F.; Chen, Z. G.; Lu, G. Q.; Cheng, H. M. *Chem. Mater.* **2008**, *20*, 7195.
(36) Wu, Z.-S.; Ren, W. C.; Xu, L.; Li, F.; Cheng, H. M. *ACS Nano* **2011**, *5*, 5463.
(37) Wen, Y. Y.; Wang, B.; Huang, C. C.; Wang, L. Z.; Hulicova-Jurcakova, D. *Chem.-Eur. J.* **2015**, *21*, 80.
(38) Hulicova-Jurcakova, D.; Puziy, A. M.; Poddubnaya, O. I.; Suarez-Garcia, F.; Tascon, J. M. D.; Lu, G. Q. *J. Am. Chem. Soc.* **2009**, *131*, 5026.
(39) Huang, C. C.; Puziy, A. M.; Sun, T.; Poddubnaya, O. I.; Suarez-Garcia, F.; Tascon, J. M. D.; Hulicova-Jurcakova, D. *Electrochim. Acta* **2014**, *137*, 219.
(40) Deng, W. F.; Zhang, Y. J.; Yang, L.; Tan, Y. M.; Ma, M.; Xie, Q. J. *RSC Adv.* **2015**, *5*, 13046.
(41) Zhang, J. L.; Jiang, M.; Xing, L. B.; Qin, K.; Liu, T. Z.; Zhou, J.; Si, W. J.; Cui, H. Y.; Zhuo, S. P. *Chin. J. Chem.* **2016**, *34*, 46.
(42) Chen, X.; Chen, X. H.; Xu, X.; Yang, Z.; Liu, Z.; Zhang, L. J.; Xu, X. J.; Chen, Y.; Huang, S. M. *Nanoscale* **2014**, *6*, 13740.
(43) Hulicova-Jurcakova, D.; Seredych, M.; Lu, G. Q.; Bandosz, T. J. *Adv. Funct. Mater.* **2009**, *19*, 438.
(44) Ai, W.; Luo, Z.; Jiang, J.; Zhu, J.; Du, Z.; Fan, Z.; Xie, L.; Zhang, H.; Huang, W.; Yu, T. *Adv. Mater.* **2014**, *26*, 6186.
(45) Wu, Z.-S.; Winter, A.; Chen, L.; Sun, Y.; Turchanin, A.; Feng, X. L.; Müllen, K. *Adv. Mater.* **2012**, *24*, 5130.
(46) Jeon, I.-Y.; Zhang, S.; Zhang, L.; Choi, H.-J.; Seo, J.-M.; Xia, Z.; Dai, L.; Baek, J.-B. *Adv. Mater.* **2013**, *25*, 6138.
(47) Yang, Z.; Yao, Z.; Li, G. F.; Fang, G. Y.; Nie, H. G.; Liu, Z.; Zhou, X. M.; Chen, X.; Huang, S. M. *ACS Nano* **2012**, *6*, 205.
(48) Higgins, D.; Hoque, M. A.; Seo, M. H.; Wang, R. Y.; Hassan, F.; Choi, J. Y.; Pritzker, M.; Yu, A. P.; Zhang, J. J.; Chen, Z. W. *Adv. Funct. Mater.* **2014**, *24*, 4325.
(49) Zhi, L. J.; Müllen, K. *J. Mater. Chem.* **2008**, *18*, 1472.
(50) Li, X.; Song, Q.; Hao, L.; Zhi, L. *Small* **2014**, *10*, 2122.
(51) Wu, Z.-S.; Parvez, K.; Winter, A.; Vieker, H.; Liu, X.; Han, S.; Turchanin, A.; Feng, X.; Müllen, K. *Adv. Mater.* **2014**, *26*, 4552.
(52) Peng, Z. W.; Ye, R. Q.; Mann, J. A.; Zakhidov, D.; Li, Y. L.; Smalley, P. R.; Lin, J.; Tour, J. M. *ACS Nano* **2015**, *9*, 5868.
(53) Tan, Y. Z.; Osella, S.; Liu, Y.; Yang, B.; Beljonne, D.; Feng, X. L.; Mullen, K. *Angew. Chem. -Int. Ed.* **2015**, *54*, 2927.
(54) Tan, Y. Z.; Yang, B.; Parvez, K.; Narita, A.; Osella, S.; Beljonne, D.; Feng, X.; Müllen, K. *Nat. Commun.* **2013**, *4*, 2646.
(55) Vance, A. L.; Willey, T. M.; Nelson, A. J.; van Buuren, T.; Bostedt, C.; Terminello, L. J.; Fox, G. A.; Engelhard, M.; Baer, D. *Langmuir* **2002**, *18*, 8123.
(56) Yao, Y. X.; Fu, Q.; Zhang, Y. Y.; Weng, X. F.; Li, H.; Chen, M. S.; Jin, L.; Dong, A. Y.; Mu, R. T.; Jiang, P.; Liu, L.; Bluhm, H.; Liu, Z.; Zhang, S. B.; Bao, X. H. *Proc. Natl. Acad. Sci. U S A* **2014**, *111*, 17023.
(57) Deng, D.; Novoselov, K. S.; Fu, Q.; Zheng, N.; Tian, Z.; Bao, X. *Nat. Nanotechnol.* **2016**, *11*, 218.
(58) Wang, P.-I.; Pisula, W.; Mullen, K.; Liaw, D.-J. *Polym. Chem.* **2016**, *7*, 6211.
(59) Maghsoumi, A.; Narita, A.; Dong, R. H.; Feng, X. L.; Castiglioni, C.; Mullen, K.; Tommasini, M. *Phys. Chem. Chem. Phys.* **2016**, *18*, 11869.
(60) Tucek, J.; Blonski, P.; Sofer, Z.; Simek, P.; Petr, M.; Pumera, M.; Otyepka, M.; Zboril, R. *Adv.Mater.* **2016**, *28*, 5045.
(61) Ma, Z.; Dou, S.; Shen, A.; Tao, L.; Dai, L.; Wang, S. *Angew. Chem. -Int. Ed.* **2015**, *54*, 1888.
(62) Sheng, K. X.; Sun, Y. Q.; Li, C.; Yuan, W. J.; Shi, G. Q. *Sci. Rep.* **2012**, *2*, 247.
(63) Ghosh, A.; Le, V. T.; Bae, J. J.; Lee, Y. H. *Sci. Rep.* **2013**, *3*, 2939.
(64) Miller, J. R.; Outlaw, R. A.; Holloway, B. C. *Science* **2010**, *329*, 1637.
(65) Yang, X. W.; Cheng, C.; Wang, Y. F.; Qiu, L.; Li, D. *Science* **2013**, *341*, 534.
(66) Wu, Z.-S.; Liu, Z.; Parvez, K.; Feng, X.; Müllen, K. *Adv. Mater.* **2015**, *27*, 3669.
(67) Zhang, M.; Zhou, Q. Q.; Chen, J.; Yu, X. W.; Huang, L.; Li, Y. R.; Li, C.; Shi, G. Q. *Energy Environ. Sci.* **2016**, *9*, 2005.
(68) Gogotsi, Y.; Simon, P. *Science* **2012**, *335*, 167.
(69) El-Kady, M. F.; Strong, V.; Dubin, S.; Kaner, R. B. *Science* **2012**, *335*, 1326.

**SYNOPSIS TOC**